MRS 50 YEARS

Recent developments in metal-based plasmonic nanomaterials

Veronica Pawlik, Shan Zhou, Dong Qin, and Younan Xia*

Since the 2005 issue on "Synthesis and Plasmonic Properties of Nanostructures" in *MRS Bulletin*, significant progress has been made with respect to the synthesis, structure–property relationship, and application of plasmonic nanomaterials. With a number of selected examples, here we provide a brief account of recent demonstrations and developments. We start with three syntheses to highlight the precision and power of chemical methods in fabricating plasmonic nanomaterials with diverse, well-defined, and controllable sizes, shapes, morphologies, and structures. We then showcase some innovative applications based upon plasmonic nanomaterials, including self-assembly, plasmonic catalysis, touch-screen display, metamaterial engineering, and photothermal heating for water evaporation. Finally, we offer some perspectives on the existing challenges and opportunities in pushing plasmonic nanomaterials to the next level of success.

Introduction

Light–matter interactions play a central role in many applications, including photodetection, vision, imaging, light harvesting, photochemistry (e.g., photocatalysis and photoelectrochemical energy conversion), and photon-based theranostics.[1–3] Among these interactions, localized surface plasmon resonance (LSPR) involving metal-based nanostructures has attracted the most attention in recent years because of its extraordinary large cross section and highly tunable resonance wavelength.[4] LSPR refers to the coherent oscillation of conduction-band electrons in a plasmonic nanostructure, which is typically made of a metal or a heavily doped semiconductor (not discussed in this article). Upon excitation, the plasmon can decay through different channels, offering a range of capabilities to convert the incident light to different forms of energy.[5] Decay through the radiative channel leads to intense optical scattering, which can be applied to generate a light-trapping effect and thus enhance the absorption of light by a nearby component situated in a hetero-nanostructure. As an immediate application, the strong confinement and enhancement of local electric fields intrinsic to LSPR has been utilized to augment a variety of optical processes such as the scattering, absorption, and emission of light, as well as energy transfer between the molecular species or solid materials in proximity to the plasmonic nanostructure. In parallel, the plasmon can decay through a nonradiative channel for the initiation of various processes related to electrons, photons, and phonons. In particular, the thermal energy arising from nonradiative decay has been harvested to achieve intense and localized photothermal heating. Plasmon-induced energetic carriers (so-called hot electrons and holes) derived from the dephasing of a plasmon and subsequent nonradiative Landau damping, have also been leveraged to improve the performance of many types of light-driven devices, including photodetectors, solar cells, and photocatalytic reactors.

As an optical phenomenon, LSPR has been known since the fourth century (the Lycurgus cup[6]), with the first experimental observation documented by Faraday in 1857.[7] It has evolved into a burgeoning field of research, commonly referred to as plasmonics, that concentrates on the localization, guiding, and manipulation of electromagnetic waves beyond the diffraction limit and down to the nanometer length scale.[8] While the interactions between light and metal nanoparticles have long attracted the interest of scientists

Veronica Pawlik, School of Chemistry and Biochemistry, Georgia Institute of Technology, Atlanta, USA; vpawlik3@gatech.edu
Shan Zhou, Department of Nanoscience and Biomedical Engineering, South Dakota School of Mines & Technology, Rapid City, USA; shan.zhou@sdsmt.edu
Dong Qin, School of Materials Science and Engineering, Georgia Institute of Technology, Atlanta, USA; dong.qin@mse.gatech.edu
Younan Xia, School of Chemistry and Biochemistry, Georgia Institute of Technology, Atlanta, USA; School of Chemical and Biomolecular Engineering, Georgia Institute of Technology, Atlanta, USA; younan.xia@bme.gatech.edu
*Corresponding author
doi:10.1557/s43577-023-00592-7

since the pioneering work of Mie in 1908,[9] plasmonics represents a relatively new level of control and study that involve both nanostructures and light. Rather than deriving optical properties from metal nanostructures, interactions are now controlled to manipulate light for a specific purpose. Plasmonics is an active endeavor in nanoscience. Sophisticated models, theories, and methods are constantly being developed to understand the interactions between metal nanostructures and light. Plasmonics is also part of nanotechnology because nanostructures are developed as the active components to focus, guide, and manipulate light, in addition to their use as building blocks for the construction of larger, more complex "metamaterials" sought for controlling light.

Silver (Ag) is likely the most important material in LSPR.[10] It offers many advantages over other metals (e.g., Au, Cu, Li, and Al) known to support plasmons in the visible and near-infrared regions. The ability of a material to support a plasmon is determined by its dielectric function ε, which includes real part (ε_r) and imaginary part (ε_i) both of which vary with the excitation wavelength (λ). The dielectric function of a material reflects the unique interaction between its electrons and light. A good understanding of LSPR can be found in Mie theory for calculating the extinction (absorption + scattering) cross section of a spherical nanoparticle:[9]

$$C_{ext} = \frac{24\pi^2 R^3 \epsilon_m^{3/2}}{\lambda}\left[\frac{\epsilon_i}{(\epsilon_r + 2\epsilon_m)^2 + \epsilon_i^2}\right], \quad 1$$

where C_{ext} is the extinction cross section, R is the radius, and ε_m is the relative dielectric constant of the medium surrounding the nanoparticle. This equation indicates that the interaction between a nanoparticle and light depends on its dielectric properties (ε_r and ε_i). When the denominator of the bracketed expression in the equation approaches zero, C_{ext} becomes extremely large, greatly increasing optical absorption and scattering. This is known as the resonance condition. In order to achieve this, ε_r must be close to $-2\varepsilon_m$, which can be easily met by metals such as Ag, but impossible for dielectrics and nonmetals that typically have ε_r values between 1 and 50.

The surface plasmon strength (or damping) for LSPR can be gauged using the quality factor (Q):[11]

$$Q = \frac{\omega(d_r/d\omega)}{2(\epsilon_i)^2}. \quad 2$$

The strength of a surface plasmon is directly proportional to Q. A large value of Q corresponds to a strong plasmon whereas a small value indicates a lossy or weak plasmon marked by a small C_{ext}. In general, Q should be greater than ~10 for most plasmonic applications; however, the most appropriate performance metric depends strongly on the desired application.[12] According to the plot in **Figure 1**, Ag has the largest quality factor across most of the spectrum (300–1200 nm). In contrast, Al is only suitable for applications in the ultraviolet region. Interband transitions also play a vital role in dampening surface plasmons. Typically, such transitions take place at much higher frequencies than those of LSPR, as in the case of Ag. For Au and Cu, however, these transitions limit their LSPR modes to wavelengths longer than 500 and 600 nm, respectively.

Precision nanostructures for plasmonics

The last two decades have witnessed the successful implementation of seed-mediated growth as a simple and powerful route to the production of plasmonic nanostructures with well-defined and controllable compositions, sizes, shapes, morphologies, and internal structures.[13] This synthetic approach is built upon the concept that nanocrystals with a uniform size, controlled shape, and well-defined internal structure can serve as seeds for the heterogeneous nucleation and overgrowth of the same or a different metal to generate larger and/or more complex nanocrystals. As a major advantage over the conventional methods involving homogeneous nucleation, seed-mediated growth allows for an exquisite control over the size of resultant nanocrystals by simply varying the ratio of the seeds to the added salt precursor. Further, with proper kinetic control, one can also precisely maneuver the shape or morphology taken by the resultant nanocrystals, as well as noticeably increase the scalability of the synthesis.

Nanospheres have long been sought for fundamental studies as their plasmonic properties can be exactly calculated by solving Maxwell's equations, as first demonstrated by Mie.[9] The synthesis of Au nanoparticles with a pseudospherical shape dates back to 1951 when Turkevich reported a simple and robust method based on citrate reduction.[14] Despite their great promise as a model system for plasmonic studies and building blocks for self-assembly, Au nanoparticles with a truly spherical shape and well-controlled sizes over a broad range remained a synthetic challenge until a seed-mediated method was reported in 2014.[15] The new method allows for the synthesis of single-crystal Au nanospheres with a uniform diameter tunable in the range of 5–150 nm. The synthesis starts with the preparation of Au clusters through the rapid reduction of a Au(III) precursor in the presence of a strong reducing agent such as $NaBH_4$. The Au clusters then serve as seeds for overgrowth through the reduction of dropwise-added Au(III) precursor by ascorbic acid (H_2Asc). By controlling the amount of Au(III) precursor relative to the number of Au clusters involved, the diameter of the Au nanosphere can be precisely tuned in the range of 5–16 nm (**Figure 2**a–b). Sequential seed-mediated growth with dropwise addition of Au(III) precursor solution are conducted using the 10-nm Au nanospheres as seeds to obtain nanospheres with diameters in the range of 15–80 nm (Figure 2c–d), and 46-nm nanospheres as seeds to obtain nanospheres with larger diameters

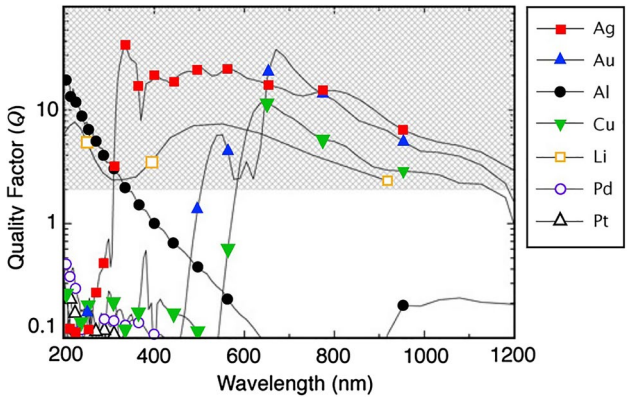

Figure 1. The quality factor (*Q*) of the localized surface plasmon resonance involving a metal/air interface. A higher *Q* denotes less damping and a stronger plasmon resonance. The shaded area represents the region of interest for many applications. Reprinted with permission from Reference 11. © 2009 Elsevier.

of 70–150 nm (Figure 2e–f). As a result of the moderate precursor injection rate for growth and a relatively low concentration of the reducing agent, a perfect spherical shape is preserved for the Au nanospheres. The Au nanospheres exhibit a major LSPR peak around 520 nm, which slightly shifts and broadens upon increasing particle size. These Au nanospheres can serve as seeds to grow nanocrystals with uniform sizes and diverse shapes, including the Au tetrahedral nanocrystals discussed later.

In another example of seed-mediated growth, penta-twinned Ag nanorods with tunable aspect ratios were synthesized.[16] The optical response of a plasmonic nanostructure is highly dependent on its geometric shape and physical dimensions. To this end, the aspect ratio of one-dimensional (1D) nanostructures offers a tunable knob for controlling their LSPR peak position. Nanorods are particularly attractive as they can support two distinct LSPR modes, transverse and longitudinal, with the latter being strongly dependent on the aspect ratio of length to diameter.[17] To create a nanorod without plasmonic resonances in the visible region (approx. 400–800 nm), the diameter, responsible for the transverse mode, must be small enough to generate a peak under 400 nm while the length must be long enough to push the longitudinal resonance beyond 800 nm. Controlling the diameter and length independently can be challenging in a one-pot synthesis so a seed-mediated protocol was developed. Although Ag nanorods have been successfully grown from both Ag and Au seeds,[17,18] the Ag seeds could not be reliably synthesized at sizes small enough while the Au seeds have their own plasmonic resonances in the visible region. In addressing this issue, we chose Pd decahedral nanocrystals as the seeds for their small size and lack of plasmon resonance in the visible region. **Figure 3**a–b shows a high-angle annular dark-field (HAADF) scanning transmission electron microscopy (STEM) image alongside the corresponding energy-dispersive x-ray spectroscopy (EDX) mapping of the Pd–Ag nanorods. The EDX clearly supports the schematic depiction of the suggested asymmetric growth mechanism depicted in Figure 3c, which was induced through slow kinetics and lattice mismatch. As the nanorods increased in length, the longitudinal plasmon mode was red-shifted. The simplest proxy for this was to control the reaction time as shown

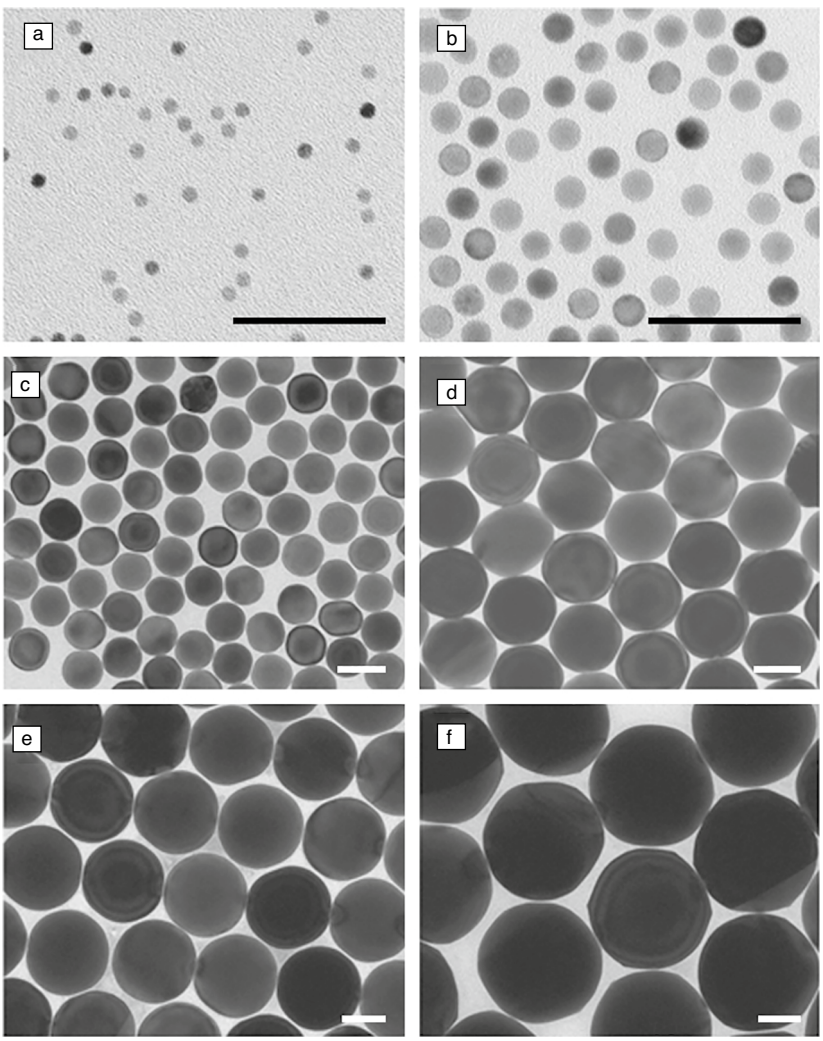

Figure 2. Transmission electron microscope images of Au nanospheres with uniform diameters precisely controlled in the range of 5–150 nm. Specifically, the images correspond to (a) 5 nm, (b) 10 nm, (c) 46 nm, (d) 80 nm, (e) 100 nm, and (f) 150 nm Au nanospheres. Scale bars = 50 nm. Reprinted with permission from Reference 15. © 2014 Wiley.

in Figure 3d–e. The photograph in Figure 3d gives a clear visual reflection of the corresponding extinction spectra in Figure 3e. It is clear from the spectra that the peak position of the transverse mode does not shift while the longitudinal mode red-shifts as the aspect ratio is increased, giving a clear path to creating Ag nanorods without plasmon resonance in the visible spectrum. Such nanorods would find immediate use in the fabrication of conductive, transparent, and flexible electrodes sought for in touch screens and related applications as discussed later.

Plasmonic nanostructures can be further enhanced through the incorporation of more complex designs such as core–shell or core–frame configurations. Careful selection of components can provide enhanced stability and introduce catalytic activity, or even alter and enrich plasmonic characteristics.[19] To this end, Ag provides a particularly interesting, but challenging system for the synthesis of core–shell or core–frame nanostructures. Because of its distinctly low reduction potential (0.79 V), Ag is especially prone to galvanic replacement.[20] Galvanic replacement is a spontaneous electrochemical process that takes advantage of the difference in electrochemical potentials between two metals. This process reduces the more noble metal at the expense of the already reduced, lower potential metal. The mechanism is so simple that often it only requires that an appropriate metal precursor is added to presynthesized seeds as is the case for Au-based nanocages (AuNCs) derived from Ag nanocubes.[21] However, because galvanic replacement necessarily requires the sacrifice of the less noble metal, products are typically hollow or exhibit rough and pitted surfaces. To avoid these pitfalls, creative synthetic solutions have been implemented to avoid galvanic replacement.[22] **Figure 4** shows the schematics of two leading strategies. The top pathway takes advantage of manipulating the reduction rate.[23] Adding NaOH increases the pH of the reaction to 11.9, which ensures that the reducing agent, H_2Asc, is actually in the diascorbate form to increase the reducing power. This transition allows the reduction rate of the second metal to outperform the galvanic replacement rate. Final morphology is dependent upon the amount of the second metal added and can result in core–frame and core–shell structures, as well as nanoframes and nanoboxes depending on subsequent steps.

Alternatively, the bottom pathway utilizes Le Chatelier's principle.[24] Galvanic replacement was avoided by co-titrating Ag^+ ions alongside a second metal at a slow reduction rate. Again, reduction strength was manipulated, this time by lowering the pH. In this case, both Ag and the second metal are codeposited on the presynthesized Ag nanocubes simultaneously. The resulting morphologies are similar to those described for the previous method with the exception of the core–shell structure and nanoboxes, which are not possible to form because the "shell" layer would be composed of an alloy of Ag and the second metal.

Self-assembly of plasmonic nanostructures

Self-assembly is an attractive strategy for constructing complex structures or ordered lattices from nanoscale building blocks to achieve plasmonic, mechanical, and catalytic properties beyond the single particle level.[25] Here, we use two examples to demonstrate the general concept, illustrating

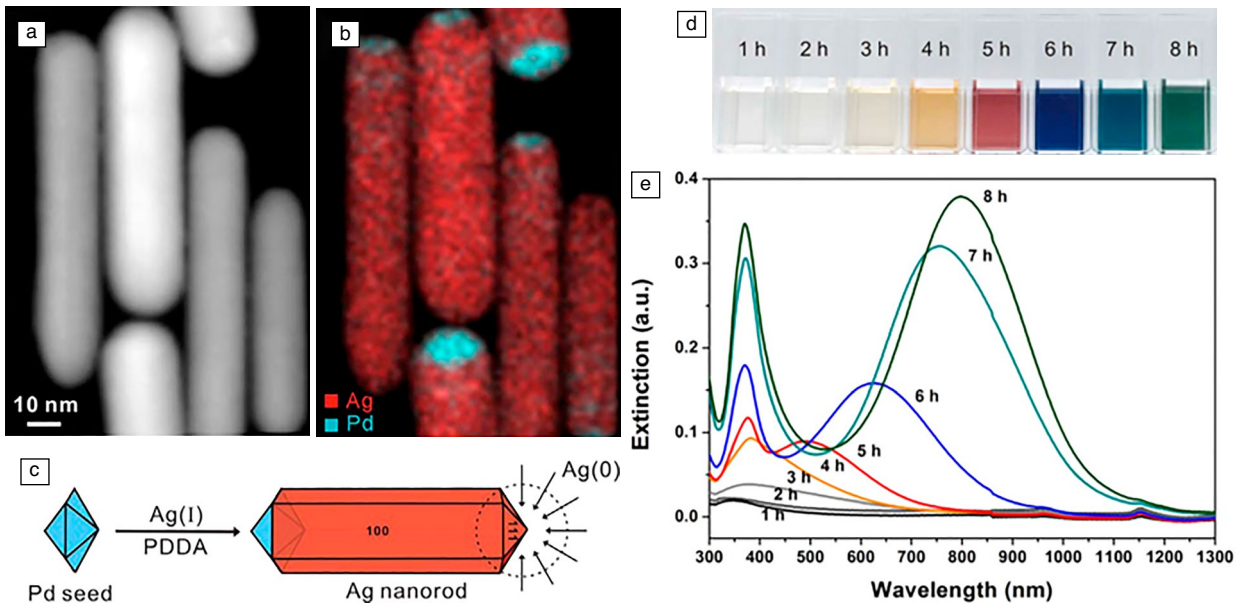

Figure 3. (a) High-angle annular dark-field-scanning transmission electron microscopy and (b) energy-dispersive x-ray spectroscopy images of Pd–Ag penta-twinned nanorods. The blue and red in (b) correspond to Pd and Ag, respectively. The 10-nm scale bar applied to both images. (c) Schematic depiction of the growth mechanism. (d) Photograph and corresponding (e) UV–vis spectra of the nanorods obtained at different reaction times. Reprinted with permission from Reference 16. © 2015 American Chemical Society.

how plasmonic nanostructures can be assembled to access new properties and applications.

The first example involves the self-assembly of Ag nanocubes into distinct structures that span from 1 to 2D and 3D.[26] Following one of the three different schemes in **Figure 5**a, different types of surface-functionalized Ag nanocubes can be prepared. Specifically, the cubic building blocks are selectively functionalized with self-assembled monolayers (SAMs) based upon hydrophobic octadecanethiol (ODT) and hydrophilic mercaptohexadecanoic acid (MHA). Depending on the exact fabrication procedure and sequence, the resultant nanocubes can have all six faces equivalent, one face different from the rest, or two identical faces on opposite sides (Figure 5a). The precise control over the number of hydrophobic and hydrophilic faces on Ag nanocubes allows them to self-assemble in water to generate distinct structures via hydrophobic attraction. For example, Ag nanocubes with six hydrophilic faces remain unassembled (Figure 5b), whereas those with one, two, and four faces functionalized with hydrophobic ODT favor the formation of dimers (Figure 5c), 1D chains (Figure 5d), and 2D sheets (Figure 5e) or star-shaped structures (Figure 5f), respectively. Complete functionalization of all six faces with ODT results in the formation of a 3D lattice (Figure 5g). The self-alignment among the building blocks in the self-assembled structures offers a great promise for generating well-defined hot spots for surface-enhanced Raman scattering (SERS) and related applications.

The second example was recently demonstrated by Chen and co-workers, when achiral Au tetrahedral nanocrystals were used as building blocks to form chiroptically active superlattices supported on substrates.[27] Non-closely packed achiral corner-sharing lattices such as perovskite structures have shown promise in transforming into chiral structures through symmetry breaking. Inspired by that, a corner-sharing bilayer lattice of Au tetrahedral

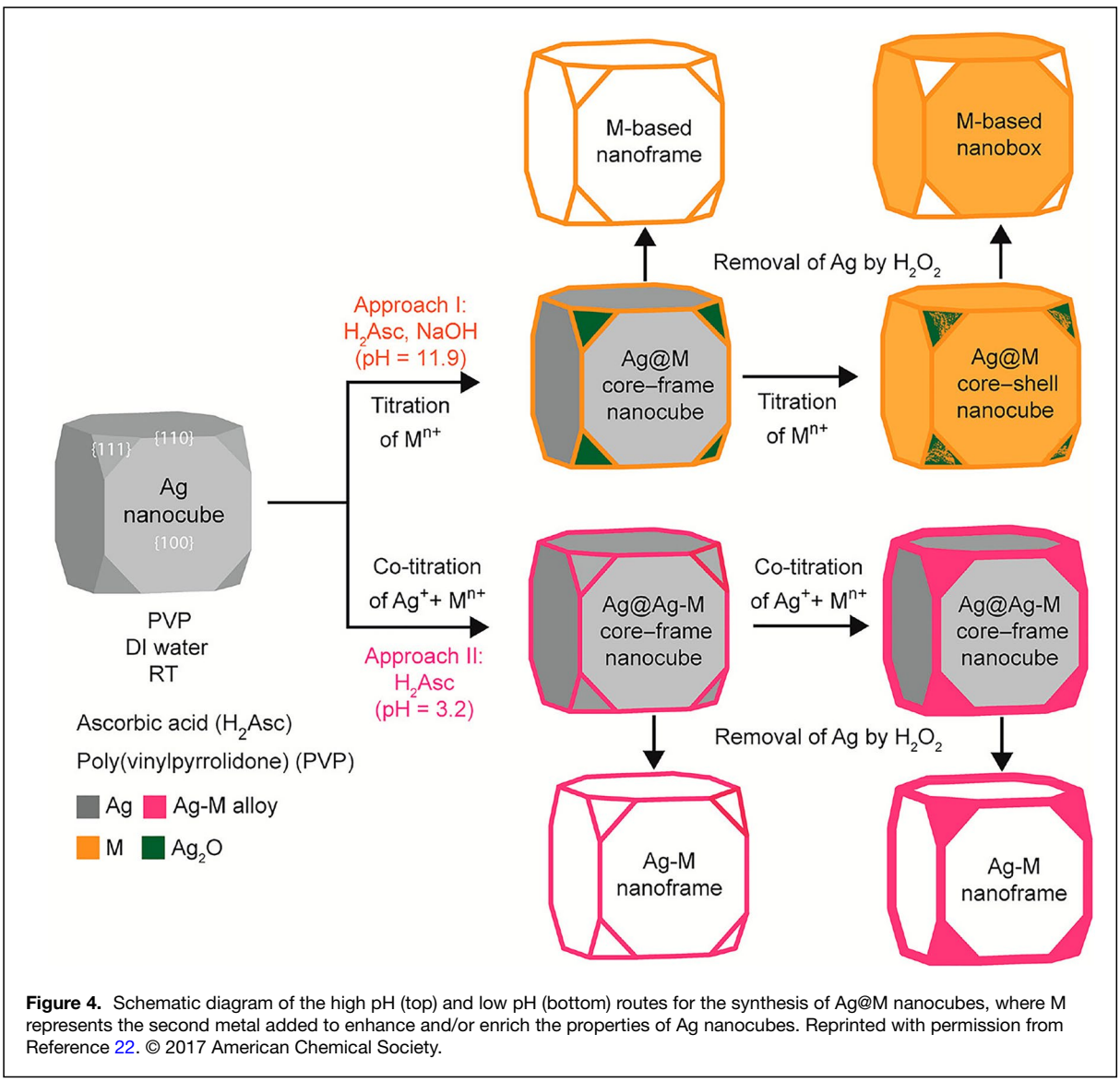

Figure 4. Schematic diagram of the high pH (top) and low pH (bottom) routes for the synthesis of Ag@M nanocubes, where M represents the second metal added to enhance and/or enrich the properties of Ag nanocubes. Reprinted with permission from Reference 22. © 2017 American Chemical Society.

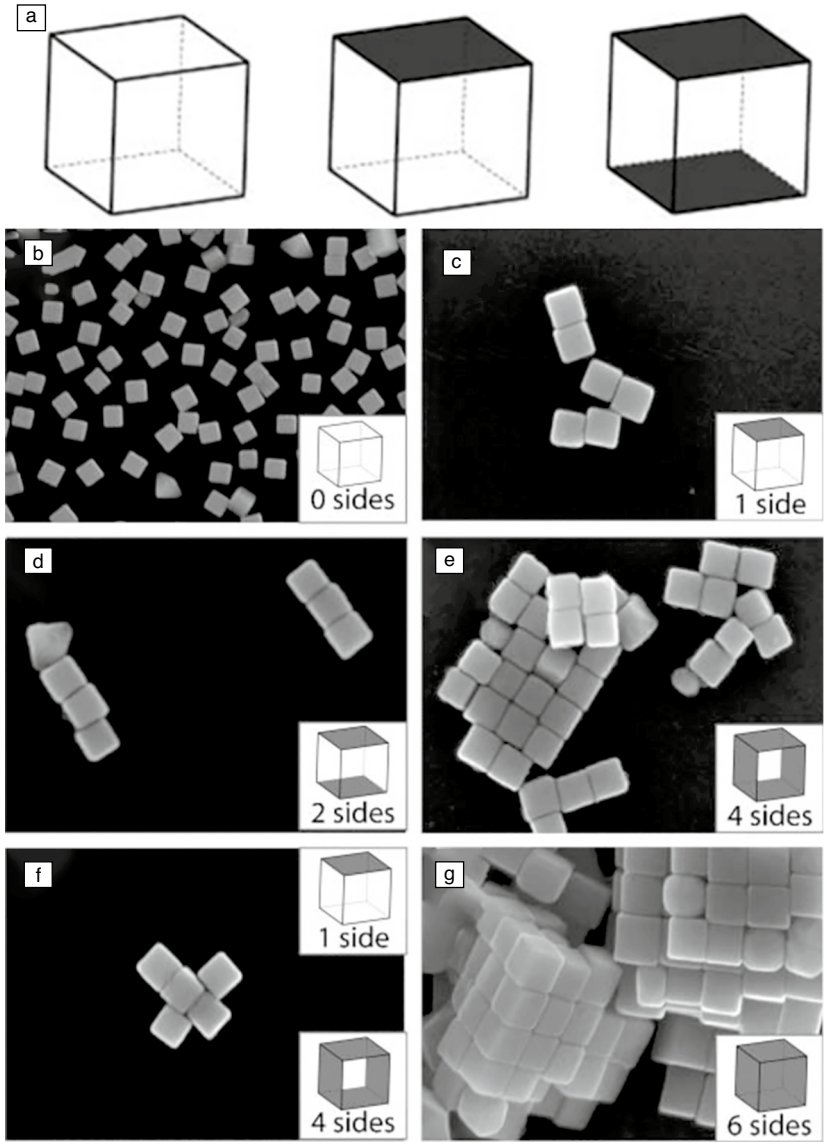

Figure 5. (a) Schematics of Ag nanocubes whose side faces are functionalized in three different ways. (b-g) Structures self-assembled from Ag nanocubes with different numbers of side faces functionalized with different combinations of hydrophilic (white color) and hydrophobic (gray color) self-assembled monolayers. The Ag nanocubes have an average edge length of 97 ± 6 nm. Reprinted with permission from Reference 26. © 2008 Wiley.

nanocrystals was fabricated on a solid substrate through an evaporation-driven self-assembly process. When nanoscale building blocks self-assemble conventionally, strong van der Waals (vdW) interactions drive the building blocks into close contact to maximize the interaction. In the presence of charged ligands, however, surface charges on neighboring building blocks can give rise to strong electrostatic repulsion. Therefore, under a careful balance between vdW attraction and electrostatic repulsion, non-closely packed structures such as a honeycomb lattice can be achieved for the tetrahedral nanocrystals (**Figure 6**a). By introducing stronger interparticle attraction through increasing the ionic strength of the solution or increasing particle size, the assembled structure underwent symmetry breaking to achieve a chiroptically active array with structural similarity to a pinwheel (Figure 6b). This chiral assembly has an extended lateral dimension of >35 μm^2 and shows strong chiroptical activity as evidenced by experimental photon-induced near-field electron microscopy and finite-difference time-domain simulations. This simple self-assembly method and the substrate-supported chiral superlattices can potentially utilize the wide variety of synthetically available nanoparticles, facilitating bottom-up manufacturing of new types of metamaterials with unusual plasmonic and chiroptical properties.

Hot electrons and plasmonic catalysis

As discussed in the Introduction, LSPR results in large extinction of light, which can be separated into scattering and absorption. Scattering occurs when photons are absorbed and reemitted at the same wavelength, but lose directionality. Alternatively, absorption can result in a number of energy dissipating pathways, including Landau damping, which creates electron–hole pairs.[28] When brought into contact with a semiconductor, plasmonic metals can inject these generated hot electrons across the Schottky barrier to create a detectable photocurrent.[29] Although light harvesting in these heterostructures promotes catalysis by increasing the number of available electrons in the semiconductor, the efficiency of this process is inherently limited because of challenges in moving the electron over the metal–semiconductor junction. Instead, energy matching conditions can be avoided through the use of a catalytic metal. Thus, a heterostructure composed of a plasmonic metal in intimate contact with a catalytic metal can utilize the hot electrons much more efficiently.[30] The most commonly used metals for this purpose are Au and Ag alongside Pt and Pd, like in those nanostructures shown in Figure 4. Despite being plasmonically active in the visible region, Cu is typically avoided because of its proclivity

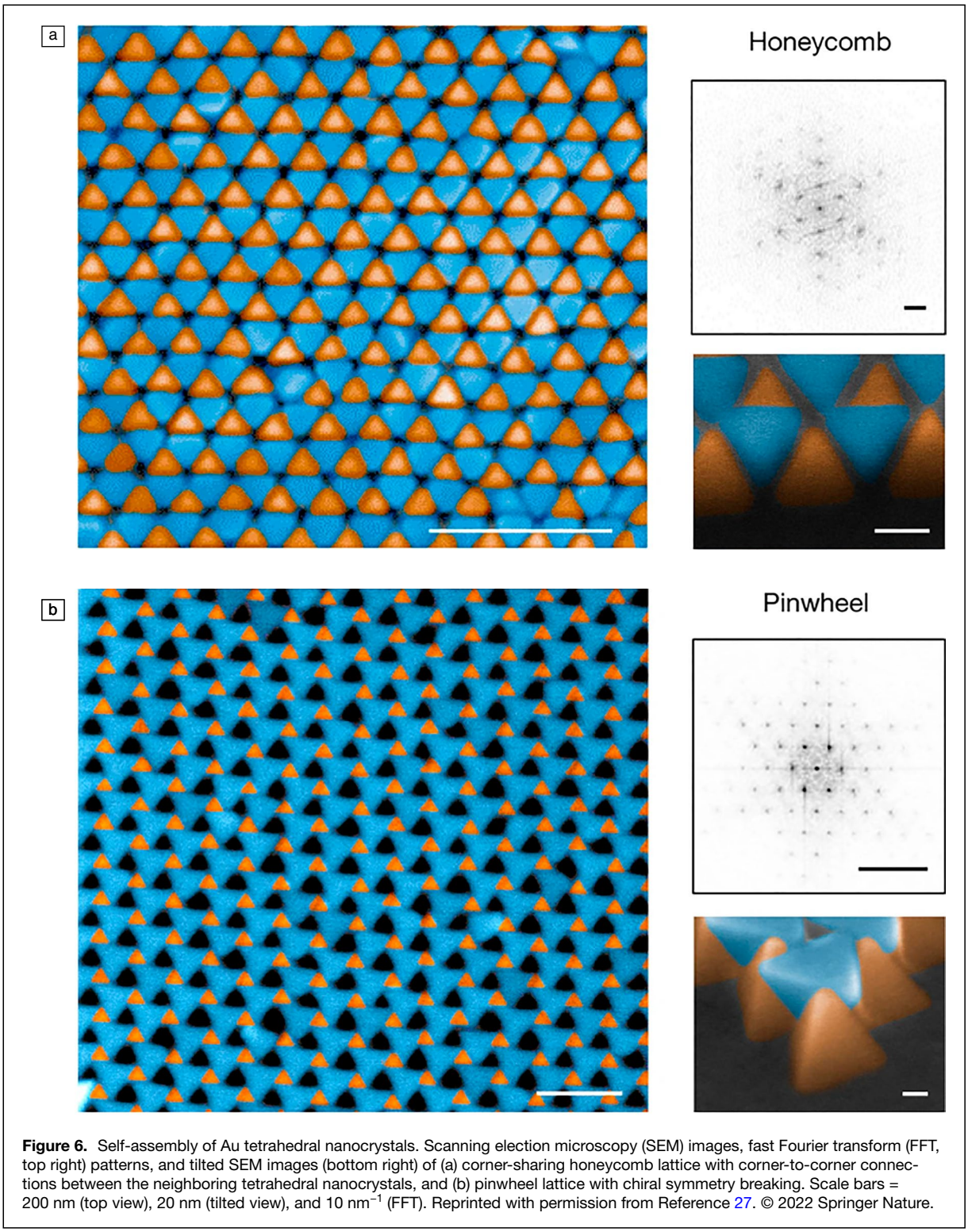

Figure 6. Self-assembly of Au tetrahedral nanocrystals. Scanning election microscopy (SEM) images, fast Fourier transform (FFT, top right) patterns, and tilted SEM images (bottom right) of (a) corner-sharing honeycomb lattice with corner-to-corner connections between the neighboring tetrahedral nanocrystals, and (b) pinwheel lattice with chiral symmetry breaking. Scale bars = 200 nm (top view), 20 nm (tilted view), and 10 nm^{-1} (FFT). Reprinted with permission from Reference 27. © 2022 Springer Nature.

to oxidize at the surface, forming a Cu_xO layer that prevents efficient hot electron transfer to the catalytic metal.[31]

Figure 7a shows finite element method simulations that depict the way in which power is dissipated over the surface of a solely plasmonic Ag nanocube and its Ag@Pt core–shell counterpart.[32] In the Ag nanocube, the plasmon decays primarily through photon scattering, which leads to a highly concentrated dissipation of power at the corners and nowhere

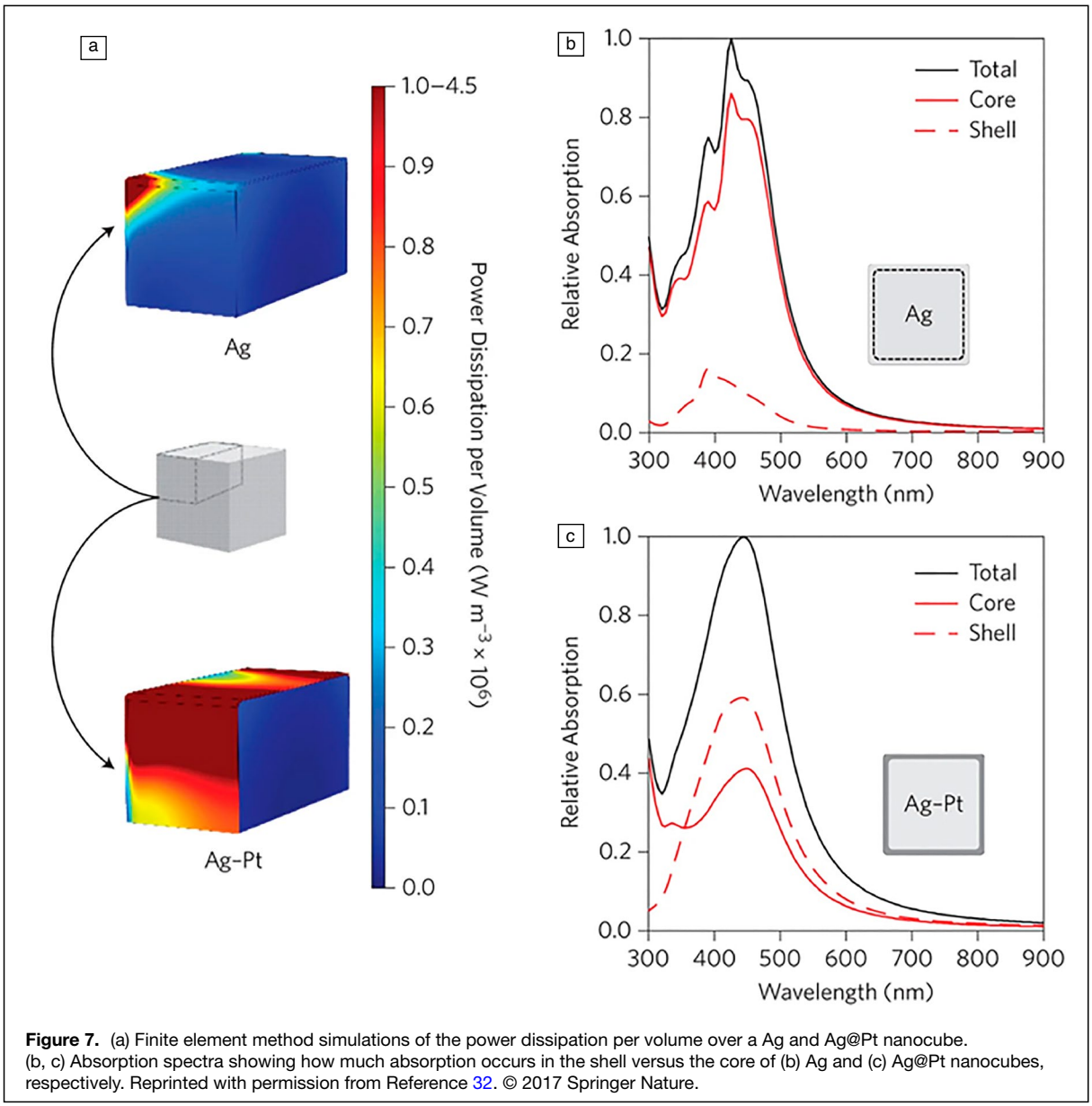

Figure 7. (a) Finite element method simulations of the power dissipation per volume over a Ag and Ag@Pt nanocube. (b, c) Absorption spectra showing how much absorption occurs in the shell versus the core of (b) Ag and (c) Ag@Pt nanocubes, respectively. Reprinted with permission from Reference 32. © 2017 Springer Nature.

else. In the Ag@Pt nanocube, however, absorption through the formation of energetic electron–hole pairs becomes the dominant decay pathway. This is because the introduction of a thin Pt shell creates a faster pathway for decay through absorption. Figure 7b–c indicates the difference in spatial distribution of absorption between the two types of particles. While absorption (and therefore energetic electron–hole pairs) is concentrated in the "shell" region of the Ag@Pt nanocube, the limited absorption in the Ag nanocube is relegated to the "core" region. Subsequent CO oxidation in the presence of excess H_2 demonstrates the significance of these decay pathways. No difference in catalytic activity was observed between Ag nanocubes that were illuminated or not, confirming the majority scattering decay pathway. Conversely, the Ag@Pt nanocubes measurably increased catalytic activity upon illumination. Similar successful light harvesting heterostructures were also utilized to catalyze a number of other reactions, including Suzuki coupling.[30]

Touch-screen display

Traditionally, indium tin oxide is used in the fabrication of transparent conductors.[33] However, its drawbacks such as cost and brittleness have motivated researchers to find suitable alternatives.[34] To this end, Ag nanowires have emerged as one of the most promising choices because of their high conductivity and tunable plasmonic peaks. As previously discussed, the positions of plasmonic peaks are strongly influenced by aspect ratios and can be easily tuned out of the visible spectrum to create highly transparent products.[16] One such application is the production of touch screens.[35] **Figure** 8a shows a schematic depiction of the final touch screen device that can not only track writing but is also force-sensitive. The dark-field optical microscopy image,

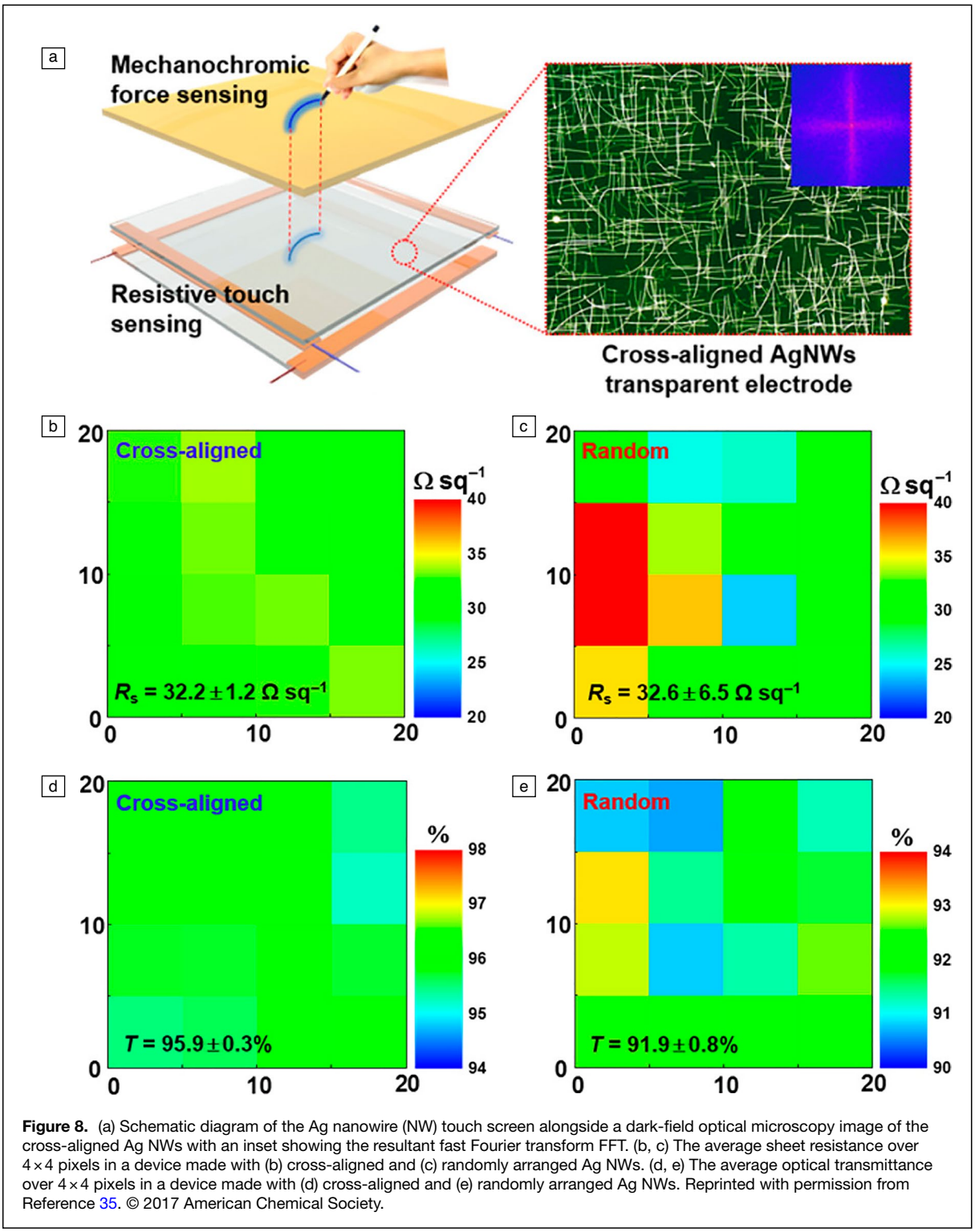

Figure 8. (a) Schematic diagram of the Ag nanowire (NW) touch screen alongside a dark-field optical microscopy image of the cross-aligned Ag NWs with an inset showing the resultant fast Fourier transform FFT. (b, c) The average sheet resistance over 4 × 4 pixels in a device made with (b) cross-aligned and (c) randomly arranged Ag NWs. (d, e) The average optical transmittance over 4 × 4 pixels in a device made with (d) cross-aligned and (e) randomly arranged Ag NWs. Reprinted with permission from Reference 35. © 2017 American Chemical Society.

alongside a FFT analysis in the inset, shows the clearly cross-aligned deposition of the Ag nanowires. This was achieved through careful use of a Meyer rod in combination with a poly-L-lysine-coated substrate. The rod ensured an even coating of Ag nanowires at an appropriate density while the poly-L-lysine increased Ag nanowire adhesion through electrostatic force. To test the success of this inexpensive aligning method, two Ag nanowire-coated substrates, one aligned and one random, were divided into 4 × 4 pixels across which sheet resistance and optical transmittance were averaged (Figure 8b–e). The

cross-aligned Ag nanowires resulted in a more even distribution of both resistance and transmittance. Further, the cross-aligned Ag nanowires outperformed the random distribution in both cases with a higher transmittance and lower sheet resistivity.

Metamaterial surfaces

Metamaterial refers to an artificially engineered material capable of manipulating the flow of waves through itself and whose characteristics are derived from structure rather than any inherent properties of its components.[36] Specifically, careful and precise engineering of a metamaterial can alter both the electric permittivity (ε) and magnetic permeability (μ) of the material such that a negative refractive index is created.[37] At optical frequencies, metals already exhibit a negative permittivity, which is responsible for the lack of transmission of electromagnetic waves. However, in general, there are no natural "double negative" materials. The second half of the 20th century saw first the theoretical conceptualization of such a material and later the first proof of concept.[38] By ensuring that both permittivity and permeability were negative, Maxwell's equations could be solved to show that an electromagnetic wave would propagate through a material in a direction opposite to that of the flow of energy.[39] This results in a negative refractive index due to the phase of the electromagnetic parameters as shown next.[36]

$$n = \sqrt{(-\mu_r)(-\epsilon_r)} = \left(\mu_r\left(e^{-j\pi}\right)\epsilon_r\left(e^{-j\pi}\right)\right)^{\frac{1}{2}} = \mu_r\left(e^{-\frac{j\pi}{2}}\right)\epsilon_r\left(e^{-\frac{j\pi}{2}}\right) = \sqrt{(\mu_r)(\epsilon_r)}e^{-j\pi} < 0 \quad (3)$$

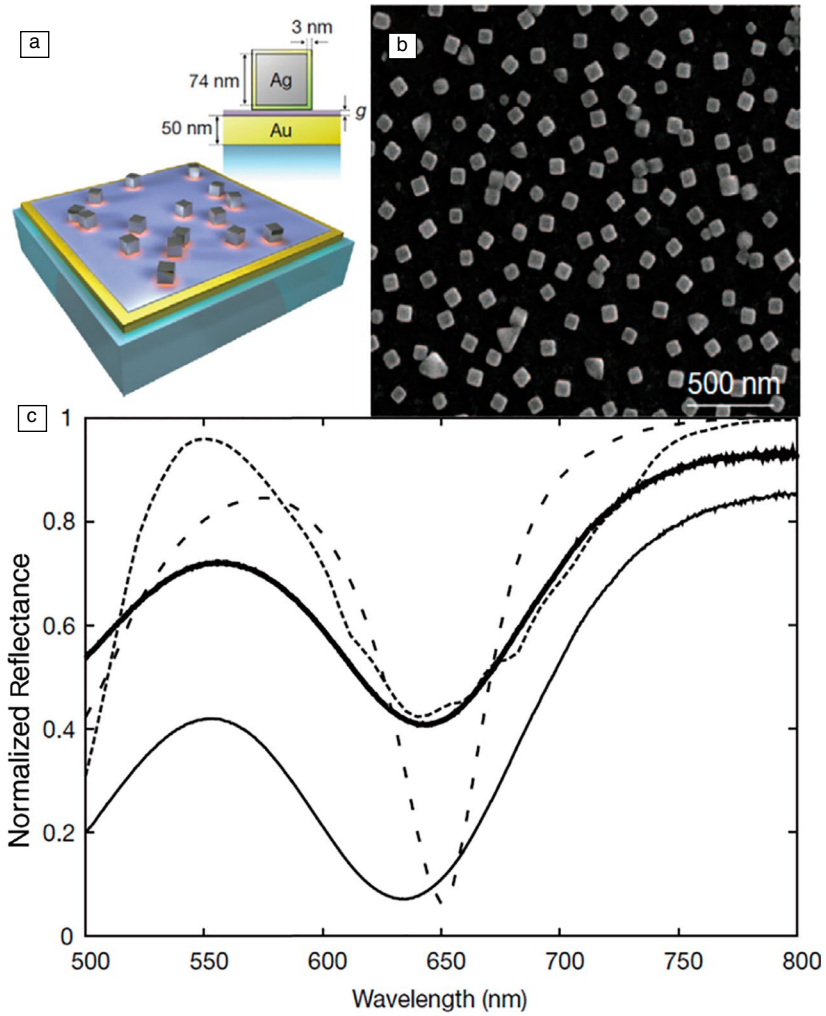

Figure 9. (a) Schematic diagram of the metamaterial surface design with inset depicting measurements for all components. (b) Scanning electron microscopy image of the chemically synthesized Ag nanocubes. (c) Reflectance spectra of the metamaterials: experimental (solid lines) and simulated (broken lines). The solid lines show the reflectance of surfaces covered with 7.3% (thin) and 17.1% (thick) Ag nanocubes. The broken lines show expected reflectance of surfaces with 4.2% (dotted) coverage and size disperse Ag nanocubes (dashed). Reprinted with permission from Reference 43. © 2012 Springer Nature.

Although metamaterials are defined by their micro and nanoscale structures, they are not completely agnostic toward the properties of their components. Because surface plasmons determine light propagation at the medium/material interface through the coupling of free electrons and photons, plasmonic materials, specifically metals, are commonly used in metamaterials.[40]

Although metamaterials have found many applications such as cloaking and antennas, total absorption/controlled reflectance has been particularly popular.[41–44] One of the greatest challenges in creating metamaterials is achieving the precise structure necessary for the desired properties. In the case of total absorption, this has usually been achieved through lithographically patterned structures,[45] making production of large metamaterial surfaces difficult and expensive. However, regular and precise patterning is not strictly necessary. As such, colloidally synthesized nanoparticles can be randomly dispersed at a minimum density across a metal film with an insulating polymer spacer to achieve matched wave impedance.[43] **Figure 9**a depicts the schematic illustration of a device where each Ag nanocube functions as a grounded patch antenna. Figure 9b shows a corresponding SEM image of the Ag nanocubes. To create total absorption, both the electric and fictitious magnetic current densities excited by an incident wave must be exactly equal, which can be achieved by varying the thickness of

the polymer spacer. This ensures that the reflected waves, which are exactly out of phase, will cancel out. Figure 9c compares the experimental and computational results of reflectance for various surfaces. The solid lines represent experimental results from 7.3% (thin line) and 17.1% (thick line) coverages of Ag nanocubes. The simulated results show reflectance with a coverage of 4.2% (dotted line) and size dispersion (dashed line). Ultimately, although theoretical calculations indicate that surface coverage as low as 3% is necessary for complete absorbance, the natural size dispersion of chemically synthesized Ag nanocubes requires a slightly higher coverage of 17 percent.

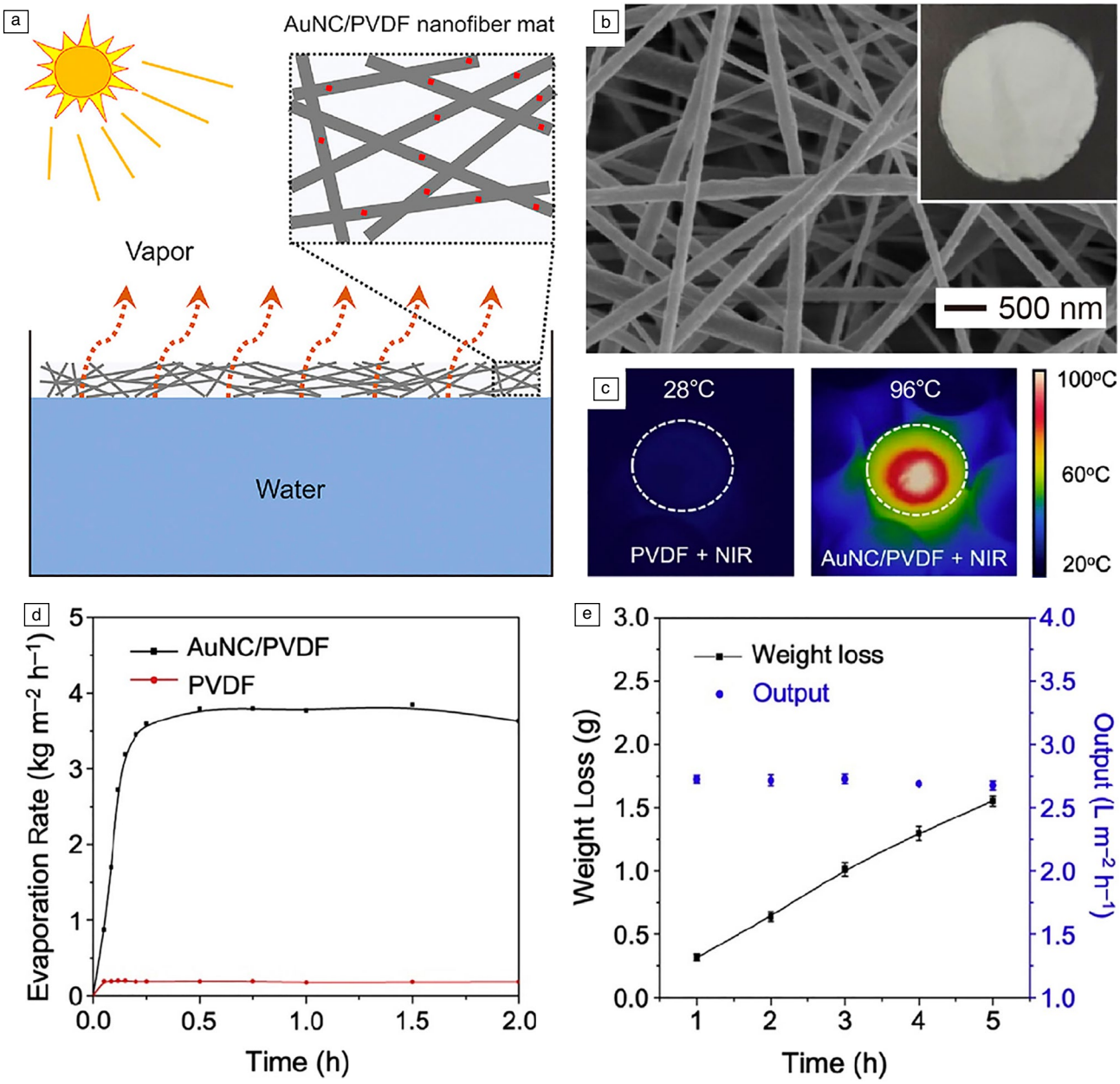

Figure 10. (a) Schematic illustration of a nonwoven mat made of AuNC/PVDF nanofibers. (b) Scanning electron microscopy image of the AuNC/PVDF nanofibers, together with a photograph of the mat in the inset. (c) Thermal images of the PVDF and AuNC/PVDF nanofiber mats after irradiation with an 808-nm laser at a power density of 0.4 W/cm^2 for 15 min. (d) The evaporation rates of the PVDF and AuNC/PVDF nanofiber mats over 2 h under laser irradiation. (e) The weight loss and rate of water output of the AuNC/PVDF nanofiber mat over 5 h under laser irradiation. Reprinted with permission from Reference 48. © 2019 Elsevier. NIR, near-infrared; NC, nanocage.

Photothermal heating and water evaporation

If the hot electrons generated through plasmon excitation are not funneled toward further surface chemistry, they can decay thermally. This thermal energy can be harvested for niche applications such as water desalination and purification. Techniques such as reverse osmosis and water boiling play a vital role in providing clean water. However, both methods traditionally require large amounts of energy. In the case of steam harvesting, the process can be energy-intensive and inefficient because it requires that the entire volume of water is brought to a boil despite vaporization only occurring at the surface.[46] The unique properties of nanomaterials have offered various strategies such as volumetric, localized, and molecular heating to mitigate this obstacle. Plasmon-induced exciton decay in plasmonic nanomaterials can be used in these strategies to more efficiently vaporize water in the format of photothermal heating.[47]

A few key factors for both host and plasmonic material are important to consider when designing a successful photothermal device. **Figure 10**a depicts the schematic design of such a system,[48] where Au nanocages (NCs) are incorporated into electrospun nanofibers made of poly(vinylidene fluoride) (PVDF). Because PVDF is hydrophobic, the nanofiber mat easily floats on top of the water. This ensures that heating only occurs at the air–water interface instead of throughout the bulk, saving energy. Figure 10b shows an SEM image of the AuNC/PVDF nanofiber mat, with the inset giving a photograph of the actual mat (approx. 1.3 cm in diameter). The SEM image clearly shows the high porosity of the nonwoven mat, which serves two purposes. The fibrous structure enables capillary action to draw water upward, away from the surface, which insulates the bulk water from the vaporizing region and increases the efficiency of heat transfer. Then, once vaporized, the open structure allows water to escape easily.

We chose AuNCs to optimize the performance of the device in a number of ways. The optical absorption of the hollow structures can be readily tuned in the visible and near-infrared (NIR) regions by controlling the wall thickness.[3] Utilizing only the outer shell of the Au nanoparticles also helps reduce the cost by eliminating the unusable core. A mixture of AuNCs in three sizes was used to cover both the visible and NIR spectra to further improve absorption of solar light. Figure 10c shows the surface temperatures of the PVDF and AuNC/PVDF nanofiber mats on water after irradiation with a NIR laser at 808 nm at a power density of 0.4 W/cm^2 for 15 min. The PVDF nanofiber mat showed minimal heating indicating the heating of the AuNC/PVDF mat should be mainly attributed to the photothermal conversion of the AuNCs. Significantly, heating was largely confined to the surface of the mat. Figure 10d–e indicates the evaporation rate, as well as weight loss and output of clean water, respectively. The evaporation rate of the AuNC/PVDF mat quickly rose to 3.64 ± 0.06 kg/m^{2}h within the first 15 min of laser irradiation and remained consistent for the full 2 h of exposure. To better test the practicality of the device, NaCl was added into the water to simulate desalination. Figure 10e shows that the rate of weight loss over 5 h of evaporation remained stable while the output of clean water was also retained. Testing the AuNC/PVDF nanofiber mat under regular solar irradiation yielded similar results.

Conclusion

Synthetic methods for plasmonic nanomaterials have come a long way since our last review of the subject in 2005.[1] For example, Ag nanocubes, which have been one of the most influential plasmonic materials of the past two decades, had only been synthesized for the first time three years prior.[49] Now, an entire body of literature is dedicated to them.[50] Likewise, as synthetic methods have improved, new applications have followed. In particular, seed-mediated strategies have done a lot to improve precision in synthetic control.[13] They have also provided a useful framework for creating more complex plasmonic systems with intricate shapes and/or multiple materials.[23] However, much work remains.

As a major application, SERS is a particularly sensitive characterization technique that can be greatly influenced not only by the exact shape of the plasmonic substrate, but also by the local environment.[51] Forming a periodic array of plasmonic nanostructures can increase reproducibility while enhancing signals. Certain shapes, such as nanocubes, can spontaneously self-assemble into arrays; however, long-range periodicity is not common or guaranteed. Instead, techniques like targeted surface coating or template-assisted self-assembly can be used.[52] Despite this, challenges still remain, especially in maintaining a surface clean enough for reliable SERS detection. On the other hand, a continuous challenge for implementing plasmonic nanomaterials in industrial settings is scalability. Strategies such as using inert gas coverings[53] and continuous flow reactors[54] have found success in many syntheses but are not universal solutions. Using an inert gas can prevent unwanted oxidation reactions but does not ensure uniform thermal or chemical distribution. Similarly, continuous flow reactors ensure uniform reaction conditions, but cannot accommodate precipitation, a common intermediate step in Ag nanomaterial syntheses. In general, Au, Ag, and Cu have long been the default plasmonic materials because of their activity in the visible spectrum. However, looking outside of traditionally metallic materials can offer flexibility in design and integration. Despite its tightly bound past, the future of plasmonic nanomaterials might not be strictly metallic.[55]

Acknowledgments

The preparation of this review article was supported in part by research grants from the National Science Foundation (CHE-2002653 and CHE-2105602), in addition to the startup funds from the Georgia Institute of Technology.

Conflict of interest

On behalf of all authors, the corresponding author states that there is no conflict of interest.

References

1. Y. Xia, N.J. Halas, *MRS Bull.* **30**(5), 338 (2005)
2. J.G. Smith, J.A. Faucheaux, P.K. Jain, *Nano Today* **10**, 67 (2015)
3. Y. Xia, W. Li, C.M. Cobley, J. Chen, X. Xia, Q. Zhang, M. Yang, E.C. Cho, P.K. Brown, *Acc. Chem. Res.* **44**, 914 (2011)
4. X. Lu, M. Rycenga, S.E. Skrabalak, B.J. Wiley, Y. Xia, *Annu. Rev. Phys. Chem.* **60**, 167 (2009)
5. Y.C. Zhang, S. He, W.X. Guo, Y. Hu, J.W. Huang, J.R. Mulcahy, W.D. Wei, *Chem. Rev.* **118**, 2927 (2018)
6. C. Louis, "Gold Nanoparticles in the Past: Before the Nanotechnology Era," in *Gold Nanoparticles for Physics, Chemistry and Biology*, 2nd edn. (World Scientific Publishing Europe, London, 2017), chap. 1, p. 1
7. M. Faraday, *Philos. Trans. R. Soc. London* **147**, 145 (1857)
8. S.A. Maier, *Plasmonics: Fundamentals and Applications* (Springer, New York, 2007)
9. G. Mie, *Ann. Phys.* **330**, 377 (1908)
10. M. Rycenga, C.M. Cobley, J. Zeng, W. Li, C.H. Moran, Q. Zhang, D. Qin, Y. Xia, *Chem. Rev.* **111**, 3669 (2011)
11. E.C. Le Ru, P.G. Etchegoin, "Introduction to Plasmons and Plasmonics," in *Principles of Surface-Enhanced Raman Spectroscopy* (Elsevier, Amsterdam, 2009), p. 121
12. P.R. West, S. Ishii, G.V. Naik, N.K. Emani, V.M. Shalaev, A. Boltasseva, *Laser Photon. Rev.* **4**, 795 (2010)
13. Y. Xia, K.D. Gilroy, H.-C. Peng, X. Xia, *Angew. Chem. Int. Ed.* **56**, 60 (2017)
14. J. Turkevich, P.C. Stevenson, J. Hillier, *Discuss. Faraday Soc.* **11**, 55 (1951)
15. Y. Zheng, X. Zhong, Z. Li, Y. Xia, *Part. Part. Syst. Charact.* **31**, 266 (2014)
16. M. Luo, H. Huang, S.-I. Choi, C. Zhang, R.R.D. Silva, H.-C. Peng, Z. Li, J. Liu, Z. He, Y. Xia, *ACS Nano* **9**, 10523 (2015)
17. B. Pietrobon, M. McEachran, V. Kitaev, *ACS Nano* **3**, 21 (2009)
18. D. Seo, C.I. Yoo, J. Jung, H. Song, *J. Am. Chem. Soc.* **130**, 2940 (2008)
19. K.D. Gilroy, A. Ruditskiy, H.-C. Peng, D. Qin, Y. Xia, *Chem. Rev.* **116**, 10414 (2016)
20. H. Cheng, C. Wang, D. Qin, Y. Xia, *Acc. Chem. Res.* **56**, 900 (2023)
21. X. Xia, Y. Wang, A. Ruditskiy, Y. Xia, *Adv. Mater.* **25**, 201302820 (2013)
22. Y. Wu, X. Sun, Y. Yang, J. Li, Y. Zhang, D. Qin, *Acc. Chem. Res.* **50**, 1774 (2017)
23. Y. Yang, J. Liu, Z.-W. Fu, D. Qin, *J. Am. Chem. Soc.* **136**, 8153 (2014)
24. J. Li, J. Liu, Y. Yang, D. Qin, *J. Am. Chem. Soc.* **137**, 7039 (2015)
25. M.A. Boles, M. Engel, D.V. Talapin, *Chem. Rev.* **116**, 11220 (2016)
26. M. Rycenga, J.M. McLellan, Y. Xia, *Adv. Mater.* **20**, 2416 (2008)
27. S. Zhou, J. Li, J. Lu, H. Liu, J.-Y. Kim, A. Kim, L. Yao, C. Liu, C. Qian, Z.D. Hood, X. Lin, W. Chen, T.E. Gage, I. Arslan, A. Travesset, K. Sun, N.A. Kotov, Q. Chen, *Nature* **612**, 259 (2022)
28. M.L. Brongersma, N.J. Halas, P. Nordlander, *Nat. Nanotechnol.* **10**, 25 (2015)
29. M.W. Knight, H. Sobhani, P. Nordlander, N.J. Halas, *Science* **332**, 702 (2011)
30. F. Wang, C. Li, H. Chen, R. Jiang, L.-D. Sun, Q. Li, J. Wang, J.C. Yu, C.-H. Yan, *J. Am. Chem. Soc.* **135**, 5588 (2013)
31. B. Sharma, R.R. Frontiera, A.-I. Henry, E. Ringe, R.P. Van Duyne, *Mater. Today* **15**, 16 (2012)
32. U. Aslam, S. Chavez, S. Linic, *Nat. Nanotechnol.* **12**, 1000 (2017)
33. M.H. Ahn, E.S. Cho, S.J. Kwon, *Vacuum* **101**, 221 (2014)
34. D. Huo, M.J. Kim, Z. Lyu, Y. Shi, B.J. Wiley, Y. Xia, *Chem. Rev.* **119**, 8972 (2019)
35. S. Cho, S. Kang, A. Pandya, R. Shanker, Z. Khan, Y. Lee, J. Park, S.L. Craig, H. Ko, *ACS Nano* **11**, 4346 (2017)
36. R. Ghatak, A. Gorai, "Metamaterials: Engineered Materials and Its Applications in High Frequency Electronics," in *Encyclopedia of Materials: Electronics* (Academic Press, Oxford, 2023), p. 419
37. G.V. Naik, V.M. Shalaev, A. Boltasseva, *Adv. Mater.* **25**, 3264 (2013)
38. G.V. Viktor, *Phys. Usp.* **10**, 509 (1968)
39. D.R. Smith, N. Kroll, *Phys. Rev. Lett.* **85**, 2933 (2000)
40. A. Boltasseva, H.A. Atwater, *Science* **331**, 290 (2011)
41. Y. Dong, T. Itoh, *Proc. IEEE* **100**, 2271 (2012)
42. J.B. Pendry, D. Schurig, D.R. Smith, *Science* **312**, 1780 (2006)
43. A. Moreau, C. Ciracì, J.J. Mock, R.T. Hill, Q. Wang, B.J. Wiley, A. Chilkoti, D.R. Smith, *Nature* **492**, 86 (2012)
44. T. Maurer, P.-M. Adam, G. Lévêque, *Nanophotonics* **4**, 363 (2015)
45. J. Hao, J. Wang, X. Liu, W.J. Padilla, L. Zhou, M. Qiu, *Appl. Phys. Lett.* **96**, 251104 (2010). https://doi.org/10.1063/1.3442904
46. F. Zhao, Y. Guo, X. Zhou, W. Shi, G. Yu, *Nat. Rev. Mater.* **5**, 388 (2020)
47. Y. Liu, S. Yu, R. Feng, A. Bernard, Y. Liu, Y. Zhang, H. Duan, W. Shang, P. Tao, C. Song, T. Deng, *Adv. Mater.* **27**, 2768 (2015)
48. T. Wu, H. Li, M. Xie, S. Shen, W. Wang, M. Zhao, X. Mo, Y. Xia, *Mater. Today Energy* **12**, 129 (2019)
49. Y. Sun, Y. Xia, *Science* **298**, 2176 (2002)
50. V. Pawlik, S. Zhou, S. Zhou, D. Qin, Y. Xia, *Chem. Mater.* **35**, 3427 (2023)
51. J.M. McLellan, Z. Li, A.R. Siekkinen, Y. Xia, *Nano Lett.* **7**, 1013 (2007)
52. Y. Xia, Y. Yin, Y. Lu, J.M. McLellan, *Adv. Funct. Mater.* **13**, 907 (2003)
53. Q. Zhang, C. Cobley, L. Au, M. McKiernan, A. Schwartz, L.-P. Wen, J. Chen, Y. Xia, *ACS Appl Mater. Interfaces* **1**, 2044 (2009)
54. G. Niu, M. Zhou, X. Yang, J. Park, N. Lu, J. Wang, M.J. Kim, L. Wang, Y. Xia, *Nano Lett.* **16**, 3850 (2016)
55. S. Kim, J.M. Kim, J.E. Park, J.M. Nam, *Adv. Mater.* **30**, 1704528 (2018) □

Veronica Pawlik is a doctoral candidate in the School of Chemistry and Biochemistry at the Georgia Institute of Technology. She received her BA degree in chemistry from Wellesley College in 2019, where she worked on layer-by-layer deposition of both organic and inorganic surfactants on gold nanoparticles. Her research focuses on crystal overgrowth mechanisms in mono and bimetallic systems. Pawlik can be reached by email at vpawlik3@gatech.edu.

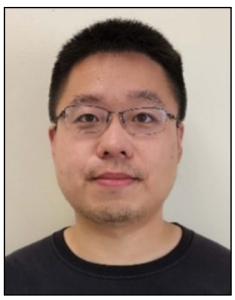

Shan Zhou has been an assistant professor in the Department of Nanoscience and Biomedical Engineering at the South Dakota School of Mines & Technology since 2022. He received his PhD degree in chemistry and biochemistry from the Georgia Institute of Technology in 2018. He completed postdoctoral research at the University of Illinois at Urbana-Champaign from 2018 to 2022. His group focuses on nanomaterial synthesis, self-assembly, and *in situ* characterization of interfaces. Zhou can be reached by email at shan.zhou@sdsmt.edu.

Dong Qin holds a faculty position in the School of Materials Science and Engineering at the Georgia Institute of Technology. She received her PhD degree in physical chemistry from the University of Pennsylvania (1996) and a MBA degree from the University of Washington (2003). She completed postdoctoral research at Harvard University from 1996 to 1997, and has held administrative positions at various institutions. She has served as an associate editor of *Nanoscale* from 2021 to 2023. Qin can be reached by email at dong.qin@mse.gatech.edu.

Younan Xia has been the Brock Family Chair and Georgia Research Alliance Eminent Scholar in Nanomedicine at the Georgia Institute of Technology since 2012. He received his PhD degree in physical chemistry from Harvard University in 1996. He started as an assistant professor of chemistry at the University of Washington in 1997 and joined Washington University in St. Louis in 2007 as the James M. McKelvey Professor of Biomedical Engineering. He served as an associate editor of *Nano Letters* from 2002 to 2019. Xia can be reached by email at younan.xia@bme.gatech.edu.